



Development of Pressure Calibration Method in High-Pressure THz ESR System

Takahiro Sakurai¹ · Yoshimasa Yasutani² · Hitoshi Sugawara² · Susumu Okubo³ · Hitoshi Ohta³

Received: 29 April 2021 / Revised: 9 July 2021 / Accepted: 12 July 2021 /
Published online: 29 July 2021

© The Author(s), under exclusive licence to Springer-Verlag GmbH Austria, part of Springer Nature 2021

Abstract

We have developed a pressure calibration method in the high-pressure THz ESR system using induction coils set outside the pressure cell. The pressure is calibrated using alternating current (AC) magnetization measurements of the superconducting transition temperature of tin set inside the pressure cell with an ESR sample. The system fits the developed pressure cell with a wide frequency range of 0.05–0.8 THz. The pressure range was extended to 2.8 GPa. The ESR system was applied to the well-known cobalt Tutton's salt $(\text{NH}_4)_2\text{Co}(\text{SO}_4)_2 \cdot 6\text{H}_2\text{O}$, and its g principal values at 0 GPa were determined as $g_1 = 6.61$, $g_2 = 3.05$, and $g_3 = 2.94$ for the first time. Furthermore, we succeeded in observing the large change in these g values with pressure.

1 Introduction

Recent progress in experimental techniques in multi-extreme environments of low temperature, high magnetic field, and high pressure has stimulated the investigation of novel quantum phenomena in condensed matter physics [1–9]. The technique in the high-pressure ESR measurement, which has been used to observe the spin states of magnetic materials under high pressure from the microscopic viewpoint, has also achieved significant progress. Since 2000, the center of its development has shifted from that in the X-band to that in the high field and high-frequency region [10–16]. ESR measurements under these multi-extreme conditions have become possible

✉ Takahiro Sakurai
tskaurai@kobe-u.ac.jp

¹ Research Facility Center for Science and Technology, Kobe University, Kobe 657-8501, Japan

² Faculty of Science, Kobe University, Kobe 657-8501, Japan

³ Molecular Photoscience Research Center, Kobe University, Kobe 657-8051, Japan

and they have revealed various interesting phenomena of quantum magnets [3, 5, 8, 17–22].

Among elemental experimental techniques, pressure calibration is a fundamental and important technique. In the measurements under multi-extreme conditions, a pressure calibration method must be established individually as physical restrictions considered differ among devices.

First, the pressure calibration methods used in low frequency high pressure ESR systems such as X-band ones will be reviewed briefly. The first high-pressure ESR system reported in 1957 was a system equipped with the so-called high-pressure bomb where oil was sent from a hydraulic pump to the sample space and pressurized directly [23]. In this system, the pressure was determined directly using the pressure gauge attached to the hydraulic pump. This is one of the most reliable pressure determination methods for measurement at room temperature, where oil does not freeze. However, this method cannot be used for measurement at liquid helium temperature.

The anvil-type cell was first introduced to ESR measurement as one of the clamp-type pressure cells in 1963 [24]. The systems that use this pressure cell have been extended to the measurement at liquid helium temperature [25, 26]. The advantages of anvil-type pressure cell are the availability of ruby fluorescence for the pressure calibration, which is suited to the anvil cells, in addition to the capability of higher pressure generation compared to piston-cylinder pressure cell [25–27]. The piston-cylinder type pressure cell was first introduced to ESR measurement in 1975 [28]. The measurement at liquid helium temperature was conducted intensively in series of experiments [28–31]. One end of the pressure cell is used as a microwave window, and the other end is used as an electrical feedthrough [29]. In these systems, indium, whose relationship between pressure and superconducting transition temperature is known, and/or manganin, whose relationship between pressure and resistance value was calibrated in advance, were used for pressure calibration. The superconducting transition temperature of indium was measured using another AC magnetization measurement system [29]. The resistance of manganin was measured by connecting wires to manganin via a feedthrough [28–31].

For ESR measurement systems available under high pressure, high field, and low temperature, there are two other systems [14, 15]. One is a system using a quasi-optical system [14], and the other is a system consisting of a resonator and a vector network analyzer [15]. In the former, a piston-cylinder type with a Poulter-type diamond window is used, and in the latter, a small plastic diamond anvil cell, which fits the resonator, is used. The pressure is calibrated by ruby fluorescence in both systems.

The above two high-pressure ESR systems observe the reflection of the microwave from the pressure cell. However, we adopted a simple transmission-type ESR to enable measurement over a wide frequency range [32]. When the piston-cylinder type pressure cell with a small outer diameter (8 mm) was used [33], the pressure was calibrated by the superconducting transition temperature of tin [34], which was set in the sample space, using a commercially available superconducting interference device (SQUID) magnetometer. To achieve sensitivity and high pressure while maintaining a wide frequency range, we developed a new piston-cylinder type

pressure cell with a relatively large sample space (5 mm) using ZrO₂-based ceramic for all internal parts [16]. This ceramic has relatively high transmittance to electromagnetic waves in the sub-THz region and has high toughness. These enable ESR measurement at a maximum pressure of approximately 2.5 GPa and a frequency range of 0.05–0.8 THz [16]. This pressure cell can be combined with various superconducting magnets, and it has been successfully combined with a cryogen-free superconducting magnet with a maximum magnetic field of 25 T [4].

However, owing to the use of ceramic, which cannot transmit visible light, the pressure calibration using a ruby scale is unavailable. Moreover, we cannot make a proper electrical feedthrough in ceramic. Since the pressure cell has a large outer diameter (25 mm), it cannot be fit in the SQUID magnetometer. Thus, it is necessary to establish a unique pressure calibration method for this high-pressure THz ESR system.

In this paper, we present a calibration method suitable for our high-pressure THz ESR system. Here the superconducting transition temperature of tin in the sample space is detected by induction coils set outside the pressure cell. The outline of the developed method will be described in Sect. 2. The AC magnetization measurement and ESR setups will be presented. In addition to the amplitude-modulation technique for the irradiated light, which is the same as the previously developed one [16], the field-modulation technique is also available in this system using the modulation coil for AC magnetization measurement. We present application examples obtained using this system in Sect. 3. Finally, we present the summary in Sect. 4.

2 Outline of System

2.1 Pressure Cells and AC Magnetization Measurement Setup

Figure 1a and b show the cross-sections of the pressure cells used in this study. The pressure cell in Fig. 1a is a previously developed one [5]. The pressure cell in b is a newly manufactured one to extend the pressure region. Both cylinders consist of an outer CuBe sleeve and an inner NiCrAl cylinder, and all internal parts are made of ZrO₂-based ceramic. The outer diameter is 23.5 mm, and the inner diameters are 5 and 4 mm for (a) and (b), respectively. The cell with an inner diameter of 5 mm shown in Fig. 1a has a maximum pressure of about 2 GPa [5]. The sample is enclosed into a Teflon capsule with the pressure-transmitting fluid Daphne 7373. By contrast, the cell with an inner diameter of 4 mm shown in Fig. 1b was confirmed to have a maximum pressure of 2.8 GPa. When the pressure above 2 GPa is needed, copper rings are required to tighten the pressure seal, as shown in Fig. 1b. Daphne 7474 with a higher solidification pressure is used as necessary. Both a tin as a pressure manometer and an ESR sample are set in a Teflon capsule. As shown in Fig. 1, a tin foil with a thickness of 0.2 mm is used and formed into a cylindrical shape to avoid interrupting the electromagnetic wave propagation. The sample is put into the tin tube.

Figure 1c schematically shows the relative position relationship between the pressure cell and the induction coils set outside the pressure cell. The pressure cell is

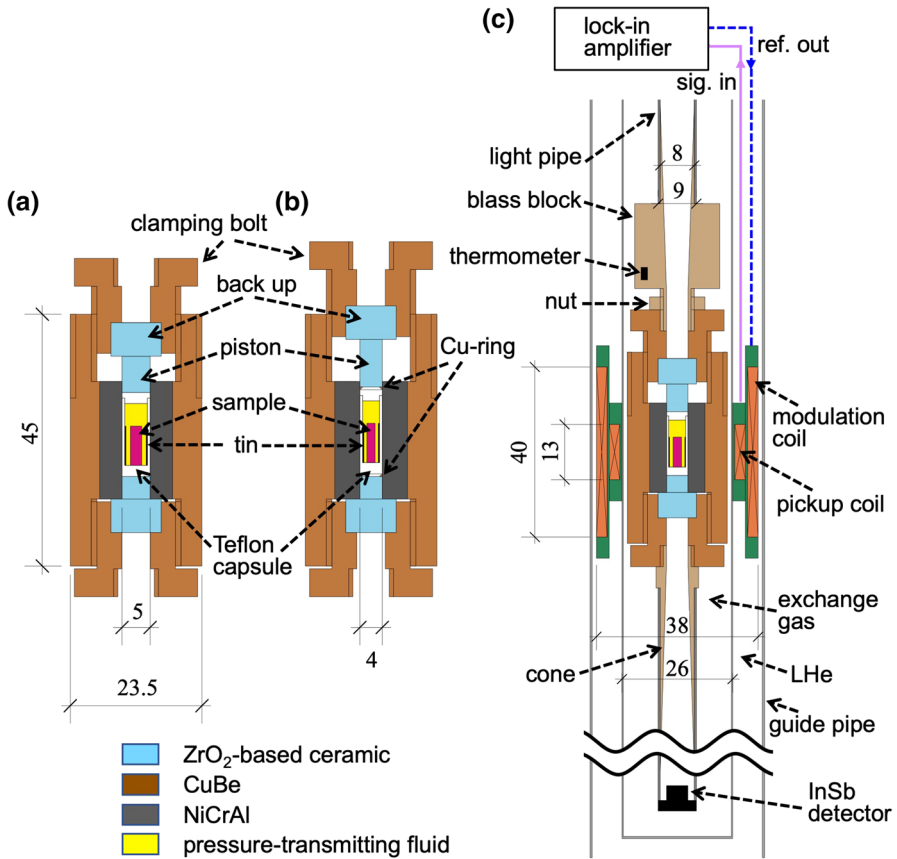


Fig. 1 Cross sections of pressure cells for high-pressure ESR measurement with inner diameters of 5 mm (a) and 4 mm (b), and a schematic of AC magnetization measurement setup (c)

connected by brass cones with a two-degree taper to light pipes with an inner diameter of 8 mm. The upper cone has a brass block, and a thermometer is embedded in this block. An InSb detector that detects the intensity of the transmitted electromagnetic wave is installed at the bottom of the lower light pipe.

The coils consist of an outside magnetic field modulation coil and an inside pickup coil. The modulation coil was made of a copper wire with a diameter of 100 μm , a number of turns of 9000, and a height of 40 mm. The pickup coil was made by a wire with a diameter of 50 μm , a total number of turns of 4900, of which the number of turns for compensation is 2600, and a height of 13 mm. These coils are fixed on a stainless pipe with an outer diameter of 26 mm to coincide exactly at their center heights. The whole probe is housed in a stainless guide pipe with an outer diameter of 40 mm. The relative position of the pressure cell is adjusted and fixed by tightening the nut so that the center of tin coincides with the centers of these coils (Fig. 1c). The space containing the pressure cell is filled with a small

amount of helium exchange gas, and the outside is in liquid helium. The temperature is controlled by pumping liquid helium. The cooling rate should be as slow as possible since the thermometer is set outside the pressure cell. It was confirmed that the superconducting transition temperature does not depend on the cooling rate if the cooling rate is approximately 100 mK/min or slower. The cooling rate was at 50 mK/min in most experiments of this study.

An induced voltage in the pickup coil is detected by a lock-in amplifier equipped with an oscillator (SR830, Stanford Research Systems, Inc.). The modulation coil is driven by this oscillator. The applied current is monitored by measuring the voltage of the resistor connected in series between the oscillator and modulation coil. The induced voltage of the pickup coil increases as the applied current or modulation frequency increases. However, this increase also raises the temperature of the pressure cell owing to the eddy current. The heating yields a temperature difference between the thermometer and tin inside the cell. As an example, we show the frequency dependence of T_c of tin. When it was measured at the fixed current 2 mA, the T_c increased to 3.708, 3.712, and 3.714 K as the frequency increased to 11, 33, and 111 Hz. This is because the Joule heat generated on the pressure cell increases as the applied frequency increases, and the outside temperature measured by the thermometer is slightly higher than the temperature inside the pressure cell which tin feels. However, when a current and frequency are several mA and 100 Hz or less, respectively, it was confirmed that the reproducibility of T_c was very high and it was obtained with an accuracy of ± 0.001 K. Therefore, if the appropriate current and frequency are applied and fixed in a series of experiments, the difference in T_c can be obtained accurately. It should be noted that it is only necessary to know the T_c difference to calibrate the pressure. Typically, the current and frequency are set at 2 mA and 33 Hz, respectively.

2.2 High-pressure ESR Measurement Setup

Figure 2 schematically shows the ESR measurement setups. The setup in Fig. 2a is similar to the previous one [16]. That is, the transmitted electromagnetic wave through the pressure cell is detected by the InSb detector. The irradiated electromagnetic wave is mechanically or electrically modulated rectangularly. The voltage of the InSb detector is detected by the lock-in amplifier using modulation frequency as a reference signal. We use a cryogen-free superconducting magnet with a maximum magnetic field of 10 T. Gunn oscillators and backward traveling wave oscillators (BWO) are used as the light source.

Figure 2b shows the setup for field-modulation type ESR measurement. In this setup, the modulation coil for the AC magnetization measurement is used, and the modulation field is applied to the sample in addition to the external field. The output current of the oscillator of the lock-in amplifier is amplified by an audio amplifier (PMA-390SE, D&M Holdings Inc.). Since the output impedance of the audio amplifier is several Ohms, while the inductance of the modulation coil is several Henry and its impedance corresponds to the order of 1 k Ω when the modulation frequency is 100 Hz, a matching transformer (TM-30T, TOA Corp.) is inserted to connect

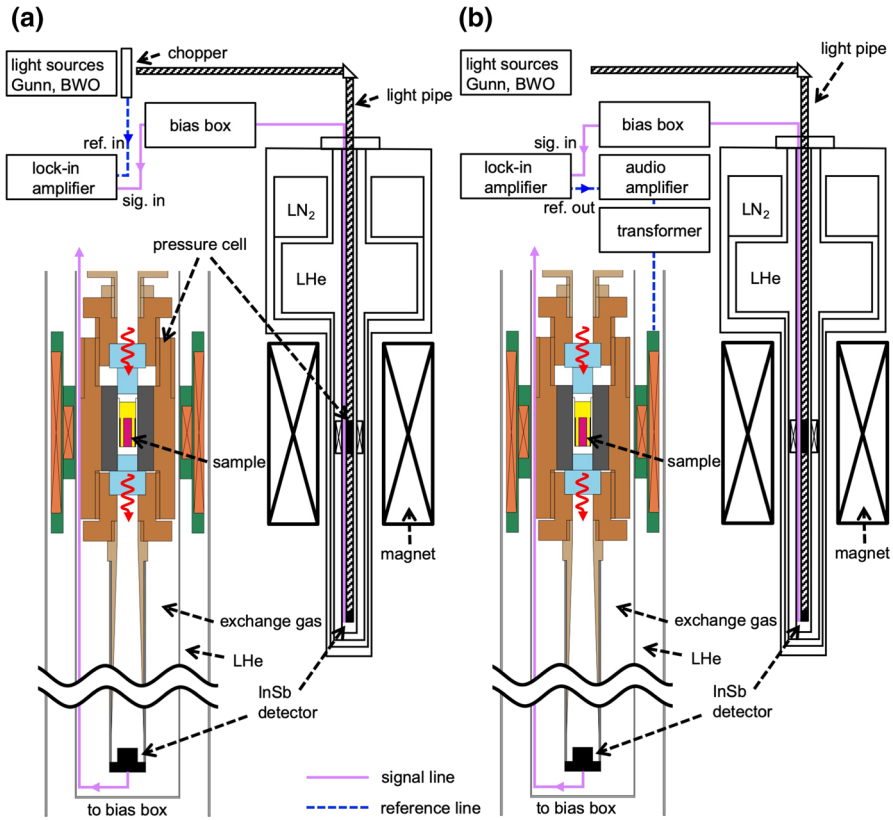


Fig. 2 Schematic diagrams for **a** transmission-type ESR measurement and **b** field-modulation-type ESR measurement

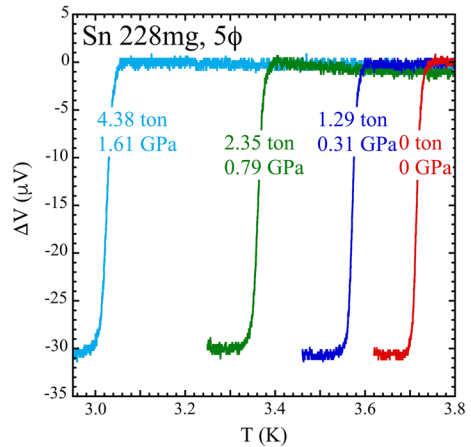
the modulation coil properly. As in the case of AC magnetization measurements, a resistor is inserted between the transformer and the coil, and the current is monitored from its voltage. A maximum current of about 200 mA can be applied. The increase of current, and thus the modulation field, enhances the signal provided that it is within the proper value as compared with the linewidth. However, as the current increases, the heating owing to the eddy current also increases. Therefore, this condition should be optimized for each sample as shown in an example in Sect. 3.2.

3 Application Examples

3.1 Pressure Calibration by AC Magnetization Measurement

The pressure cells shown in Fig. 1a and b are first loaded at room temperature, then clamped and finally attached to the device. Figure 3 shows the temperature dependence of the pickup-coil output at various loads obtained in the AC magnetization

Fig. 3 Temperature dependence of the pickup coil output at various loads for tin. The vertical axis indicates the difference ΔV from the voltage at the normal state



measurements for tin. The applied current is 2 mA, the modulation frequency is 33.3 Hz, and the amount of tin is 228 mg. A large decrease in the induced voltage was observed, indicating of the superconducting transition. The transition temperature shifted to the lower temperature side as the load is applied. The profile of the induced voltage with respect to temperature was completely reproduced at every load, indicating that no pressure inhomogeneity occurred. Besides, the temperature difference in the transition temperature ΔT_c from that at ambient pressure can be obtained by shifting the profile so that it completely coincides with the profile at ambient pressure. ΔT_c can be determined with an accuracy of ± 0.002 K, which corresponds to the pressure accuracy of ± 0.005 GPa.

As the pickup coil is not fully compensated, its induced voltage at normal state of tin is not zero and a voltage of about 2 mV remains in this experimental condition. It means that the change in induced voltage owing to the superconducting transition is about 1.5% of the total voltage for a tin of 228 mg (Fig. 3). When the amount of tin is reduced, the change becomes smaller. We confirmed that the ΔT_c can be evaluated with the same accuracy at least for a tin of 50 mg.

Figure 4 shows the relationship between the load L [ton] at room temperature and pressure P [GPa] calibrated by the following quadratic expression of pressure for tin [34].

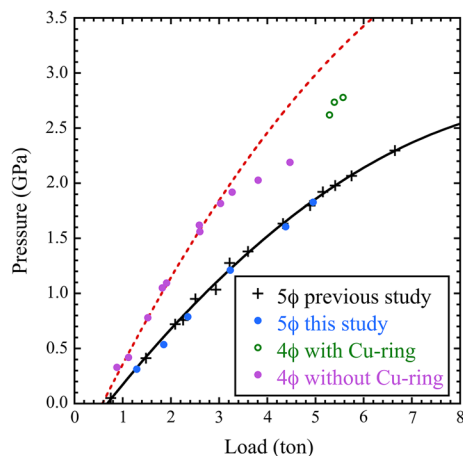
$$\Delta T_c = -4.63 \times 10^{-1} P + 2.16 \times 10^{-2} P^2. \quad (1)$$

For the results obtained in the pressure cell with the inner diameter of 5 mm, the previous result of AC magnetization measurements with small coils placed in the pressure cell (cross symbol in Fig. 4) and the fitting curve for this result (solid line in Fig. 4) [16, 35] are also plotted. The fitting curve was obtained as follows:

$$P = c + bL + aL^2, \quad (2)$$

where the parameters are given as $a = -0.0277$ [GPa/ton²], $b = 0.587$ [GPa/ton], and $c = -0.388$ [GPa] [16]. The result obtained in this study agrees with this curve

Fig. 4 Relationship between the load at room temperature and the calibrated pressure by tin. Solid and dotted lines are the fitting results by Eq. (2). See text for details



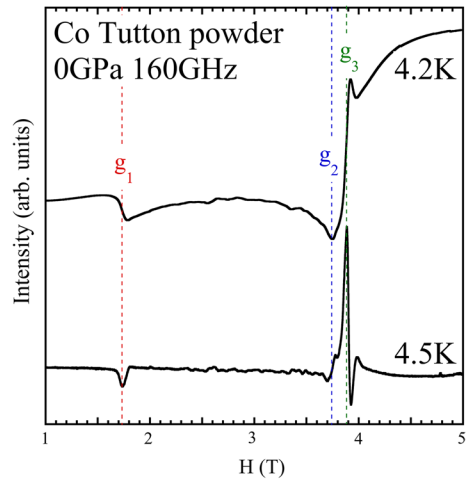
very well. This fact indicates that the pressure can be calibrated correctly using this AC magnetization measurement.

Besides, Fig. 4 shows the result of the newly manufactured pressure cell with an inner diameter of 4 mm (Fig. 1b). The dotted line is the fitting result up to 1.92 GPa with the form Eq. (2) multiplied by the cross-sectional area ratio $(5/4)^2$ with c as a free parameter. c was obtained as $c = -0.332$ [GPa]. The good agreement (Fig. 4) indicates that the pressure is properly generated in proportion to the cross-sectional area ratio up to about 2 GPa. Above 2 GPa, the pressure significantly deviated from this curve. This deviation was caused by the deformation of the cylinder. Using copper rings for the seal, it is possible to cope with this deformation; the pressure reached a pressure of 2.8 GPa (Fig. 4). However, the internal ceramic parts cracked when a higher load was applied.

3.2 Field-modulation Type ESR Measurement

The upper spectrum in Fig. 5 shows the transmission ESR spectrum obtained by the setup shown in Fig. 2a for a powder sample of typical paramagnetic salt, cobalt (Co) Tutton's salt $(\text{NH}_4)_2\text{Co}(\text{SO}_4)_2 \cdot 6\text{H}_2\text{O}$. As will be explained later, the Co Tutton salt has a large g anisotropy, and a powder pattern spread over a wide field range is observed correspondingly. The lower spectrum is a derivative ESR spectrum under the same conditions obtained using the setup in Fig. 2b, although the temperature increased slightly owing to the influence of eddy current. The applied current and modulation frequency were 20 mA and 100 Hz, respectively. They were determined as follows. For a peak of derivative spectrum at 1.7 T in Fig. 5 for instance, the S/N ratio at applied current 10 mA was about 5, and at 20 mA it became almost doubled. However, the temperature rose from 4.3 K to 4.5 K. At 40 mA, the S/N was further improved, but the temperature was further increased to 5.6 K and the peak structure around 3.8 T became unclear. This is due to the linewidth broadening by temperature increase and/or the effect that the modulation amplitude became larger than the linewidth and the spectrum deforms. As for the modulation frequency, the linewidth

Fig. 5 Powder ESR spectra of Co Tutton salt at 0 GPa and 160 GHz obtained from transmission-type ESR measurement (upper) and field-modulation-type ESR measurement (lower)



broadening due to the temperature increase was observed when the frequency was higher than 200 Hz. Based on these results, the applied current and modulation frequency were set to 20 mA and 100 Hz, respectively.

From Fig. 5, the derivative ESR spectrum was successfully obtained. The sharp peaks at the low field side (g_1) and at the high field side (g_3) on the derivative spectrum correspond to the inflection points of the transmission spectrum. A peak in the transmission spectrum (g_2) corresponds to the point where the derivative spectrum intersects the baseline. Thus, both transmission and its derivative spectra can be obtained in this ESR system.

Since the inflection point can be observed as a sharp peak using the field-modulation technique (Fig. 5), this technique is expected to be effective in investigating the pressure effect of powder samples with large anisotropy such as a metal protein with low spin density.

3.3 Pressure Effect on Cobalt Tutton's Salt

The Co Tutton's salt is a paramagnetic salt whose magnetic ion is Co^{2+} ion and has been well known for a long time. The system is described by fictitious spin $S = 1/2$ with anisotropic g values [36]. It is known that there are two nonequivalent Co ion sites in the unit cell, while the detailed crystal structure does not seem to be completely determined yet [37–39]. ESR measurements of the Co Tutton's salt were conducted intensively around the 1950s to reveal the origin of its large magnetic anisotropy [36, 40, 41]. However, to the best of our knowledge, there are few reports on the g values of Co Tutton's salt with a few exceptions [42]. This is because as there was only ESR measurement operating at low frequency at that time, such as X-band, the absorption lines from the two sites were insufficiently separated owing to its relatively broad linewidth. Bleaney et al. investigated the dilute system, where non-magnetic zinc ions in zinc Tutton's salt were replaced with Co ions by 0.1% to improve the spectral resolution in X- and K-band [41]. Thus, the g values with the

tetragonal symmetry were observed, and the g principal values were determined to be $g_{\parallel} = 6.45$, $g_{\perp} = 3.06$. It is worth noting that these g values are the g values of the dilute system, not the g values of the Co Tutton's salt itself. However, these g values have been widely used as those of Co Tutton's salt [43–45].

In this study, multi-extreme ESR measurements were performed on a powder sample of Co Tutton's salt. To the best of our knowledge, the pressure effect of Co Tutton's salt was investigated for the first time. The experiments were conducted at 4.2 K in a frequency range of 80–160 GHz with 20 GHz step and pressure range of about 2 GPa.

Figure 6 shows the pressure dependence of ESR spectra obtained at 160 GHz. The pressure is calibrated using the AC magnetization measurement in Fig. 1c. At 0 GPa, there is a shoulder structure in the peak around 3.9 T. We observed this shoulder structure above 80 GHz. It indicates that the Co Tutton's salt, which has been believed to have uniaxial anisotropy, has slight in-plane anisotropy. The octahedral crystalline field surrounding the Co^{2+} ion has been shown to have lower symmetry than tetragonal symmetry [37, 39] and this result is more consistent with its crystalline field symmetry. This was first revealed by high resolution of high field and high-frequency ESR measurement. Besides, the peak shifts to the lower field side, and the anisotropic features become pronounced as the pressure is applied. Due to insufficient grinding of the powder sample, the spectra show some structures, including the small hump seen at 3.9 T above 1.05 GPa, and they are not intrinsic.

In each spectrum, g_2 was determined from its peak, and g_1 and g_3 were determined from the peaks in its derivative line. We obtained the g principal values as $g_1 = 6.61$, $g_2 = 3.05$, and $g_3 = 2.94$ at 0 GPa. This is the first determination of the g principal values for Co Tutton's salt, as far as we know. Figure 7 shows the pressure dependence of these g values. As shown in Fig. 7, the decrease in g_1 and

Fig. 6 Pressure dependence of the ESR spectra at 160 GHz and 4.2 K obtained using transmission-type ESR measurements for Co Tutton's salt. The solid and dotted lines present the resonance positions at 0 and 1.92 GPa, respectively

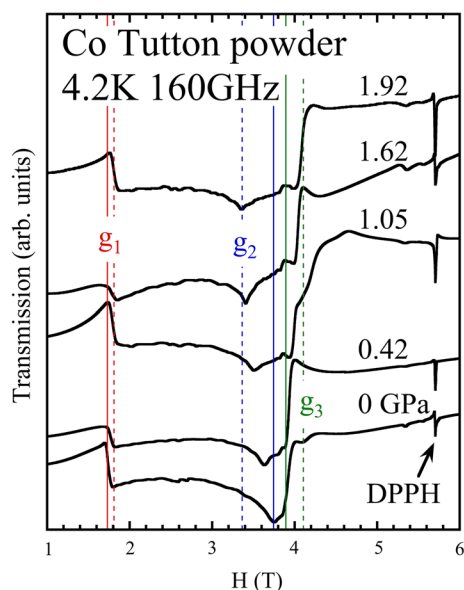
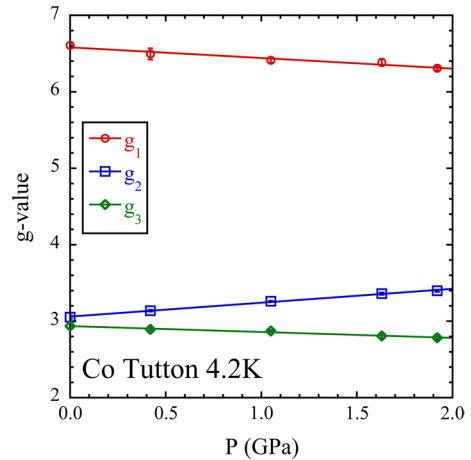


Fig. 7 Pressure dependence of g value of Co Tutton's salt at 4.2 K



g_3 , and the increase in g_2 can be seen with increasing pressure. This large pressure change in the g values is mostly caused by the deformation of the octahedral crystalline field surrounding the Co^{2+} ion. A further detailed investigation is required to understand the origin of the large pressure dependence of the g values.

4 Summary

In this study, we developed a multi-extreme ESR system equipped with induction coils for the AC magnetization measurement set outside the pressure cell. The previously developed pressure cells with ceramic internal parts for high-pressure ESR measurement can be fitted. Pressure can be calibrated by measuring the superconducting transition temperature of tin placed inside the pressure cell, and its accuracy is ± 0.005 GPa. We manufactured a new pressure cell with an inner diameter of 4 mm, which can generate a pressure of about 2.8 GPa.

In the ESR system, magnetic field-modulation type ESR measurement is possible using the modulation coil for AC magnetization measurement in addition to transmission-type ESR measurement. We applied this ESR system to a typical paramagnetic salt, Co Tutton's salt. By using a powder sample, the g principal values of Co Tutton's salt were determined for the first time. Owing to high resolution, which is an advantage of ESR measurement using high field and frequency, we obtained a slight in-plane anisotropy with respect to the g values of Co Tutton's salt at 0 GPa. Furthermore, a large pressure dependence of g values was observed for the first time.

Acknowledgements This work was supported by KAKENHI from Japan Society for the Promotion of Science: Grant Numbers 19K03746 (T.S.), and 19K21852 (H.O.). One of the authors (T.S.) would like to thank Dr. Dmytro Kamenskyi for translating the Russian paper.

References

1. S. Haravifard, D. Graf, A.E. Feiguin, C.D. Batista, J.C. Lang, D.M. Silevitch, G. Srajer, B.D. Gaulin, H.A. Dabkowska, T.F. Rosenbaum, Nat. Commun. **7**, 11956 (2016)
2. A. Sera, Y. Kousaka, J. Akimitsu, M. Sera, K. Inoue, Phys. Rev. B **96**, 014419 (2017)
3. T. Sakurai, Y. Hirao, K. Hijii, S. Okubo, H. Ohta, Y. Uwatoko, K. Kudo, Y. Koike, J. Phys. Soc. Jpn. **87**, 033701 (2018)
4. T. Sakurai, S. Kimura, M. Kimata, H. Nojiri, S. Awaji, S. Okubo, H. Ohta, Y. Uwatoko, K. Kudo, Y. Koike, J. Magn. Reson. **296**, 1 (2018)
5. R. Okuto, E. Ohki, T. Sakurai, K. Hijii, H. Takahashi, E. Ohmichi, S. Okubo, H. Ohta, Y. Uwatoko, H. Tanaka, Appl. Magn. Reson. **50**, 1059 (2019)
6. K. Sakurai, S. Kimura, S. Awaji, M. Matsumoto, H. Tanaka, Phys. Rev. B **102**, 064104 (2020)
7. J. Guo, G. Sun, B. Zhao, L. Wang, W. Hong, V.A. Sidorov, N. Ma, Q. Wu, S. Li, Z.Y. Meng, A.W. Sandvik, L. Sun, Phys. Rev. Lett. **124**, 206602 (2020)
8. T. Sakurai, B. Rubrecht, L.T. Corredor, R. Takehara, M. Yasutani, J. Zeisner, A. Alfonsov, S. Selter, S. Aswartham, A.U.B. Wolter, B. Büchner, H. Ohta, V. Kataev, Phys. Rev. B **103**, 024404 (2021)
9. H. Takeda, T. Yamauchi, M. Takigawa, H. Ishikawa, Z. Hiroi, Phys. Rev. B **103**, 104406 (2021)
10. C.P. Poole Jr., *Electron Spin Resonance* (Dover, New York, 1996), p. 337
11. S.K. Hoffmann, M. Krupski, W. Hilzner, Appl. Magn. Reson. **5**, 407 (1993)
12. T. Sakurai, S. Okubo, H. Ohta, J. Magn. Reson. **280**, 3 (2017)
13. T. Sakurai, H. Ohta, S. Hara, Y. Saito, Appl. Magn. Reson. (2020). <https://doi.org/10.1007/s00723-020-01299-7>
14. B. Náfrádi, R. Gaál, A. Sienkiewicz, T. Fehér, L. Forró, J. Magn. Reson. **195**, 206 (2008)
15. S. Hill. <https://nationalmaglab.org/user-facilities/emr/emr-measurement-techniques/high-pressure-cpr>
16. T. Sakurai, K. Fujimoto, R. Matsui, K. Kawasaki, S. Okubo, H. Ohta, K. Matsubayashi, Y. Uwatoko, H. Tanaka, J. Magn. Reson. **259**, 108 (2015)
17. T. Sakurai, M. Tomoo, S. Okubo, H. Ohta, K. Kudo, Y. Koike, J. Phys. Conf. Ser. **150**, 042171 (2009)
18. Á. Antal, T. Fehér, E. T.-Szekeres, F. Fülöp, B. Náfrádi, L. Forró, A. Jánossy, Phys. Rev. B **84**, 075124 (2011)
19. A. Prescimone, C. Morien, D. Allan, J.A. Schlueter, S.W. Tozer, J.L. Manson, S. Parsons, E.K. Brechin, S. Hill, Angew. Chem. Int. Ed. **51**, 7490 (2012)
20. K. Thirunavukkuarasu, S.M. Winter, C.C. Beedle, A.E. Kovalev, R.T. Oakley, S. Hill, Phys. Rev. B **91**, 014412 (2015)
21. T. Okamoto, E. Ohmichi, Y. Saito, T. Sakurai, H. Ohta, J. Phys. Chem. B **122**, 6880 (2018)
22. S.A. Zvyagin, D. Graf, T. Sakurai, S. Kimura, H. Nojiri, J. Wosnitza, H. Ohta, T. Ono, H. Tanaka, Nat. Commun. **10**, 1064 (2019)
23. W.M. Walsh Jr., N. Bloembergen, Phys. Rev. **107**, 904 (1957)
24. J.H. Gardner, M.W. Hill, C. Johansen, D. Larson, W. Murri, M. Nelson, Rev. Sci. Instrum. **34**, 1043 (1963)
25. N. Sakai, J.H. Pifer, Rev. Sci. Instrum. **56**, 726 (1985)
26. A. Sienkiewicz, B. Vilenó, S. Garaj, M. Jaworski, L. Forró, J. Magn. Reson. **177**, 261 (2005)
27. J.D. Barnett, S.D. Tyagi, H.M. Nelson, Rev. Sci. Instrum. **49**, 348 (1978)
28. A.Y. Kozhukhar, G.A. Tsintsadze, Phys. Lett. **55A**, 175 (1975)
29. A.Y. Kozhukhar, S.N. Lukin, G.A. Tsintsadze, V.A. Shapovalov, Cryogenics **16**, 441 (1976)
30. S.N. Lukin, G.A. Tsintsadze, Sov. Phys. JETP **42**, 128 (1976)
31. A.A. Galkin, A.Y. Kozhukhar, G.A. Tsintsadze, Sov. Phys. JETP **43**, 128 (1976)
32. H. Ohta, S. Okubo, T. Sakurai, T. Goto, K. Kiritani, K. Ueda, Y. Uwatoko, T. Saito, M. Azuma, M. Takano, J. Akimitsu, Phys. B **294–295**, 624 (2001)
33. T. Sakurai, A. Taketani, T. Tomita, S. Okubo, H. Ohta, Y. Uwatoko, Rev. Sci. Instrum. **78**, 065107 (2007)
34. T.F. Smith, C.W. Chu, Phys. Rev. **159**, 353 (1967)
35. K. Kawasaki, T. Sakurai, E. Ohmichi, S. Okubo, H. Ohta, K. Matsubayashi, Y. Uwatoko, Appl. Magn. Reson. **46**, 987 (2015)
36. B. Bleaney, D.J.E. Ingram, Nature **164**, 116 (1949)
37. H. Montgomery, Acta Cryst. **22**, 775 (1967)

38. V.G. Rau, E.N. Kurkutova, *Sov. Phys. Cryst.* **17**, 997 (1972)
39. X.-H. Li, Z.-G. Li, *Acta Cryst.* **E60**, i114 (2004)
40. A. Abragam, M.H.L. Pryce, *Proc. Roy. Soc. A* **206**, 173 (1951)
41. B. Bleaney, D.J.E. Ingram, *Proc. R. Soc. A* **208**, 143 (1951)
42. S.H. Choh, G. Seidel, *Phys. Rev.* **174**, 385 (1968)
43. N. Uryu, *J. Phys. Soc. Jpn.* **16**, 2139 (1961)
44. H.A. Farach, C.P. Poole Jr., J.M. Daniels, *Phys. Rev.* **188**, 864 (1969)
45. S. Kuroda, M. Motokawa, M. Date, *J. Phys. Soc. Jpn.* **44**, 1797 (1978)

Publisher's Note Springer Nature remains neutral with regard to jurisdictional claims in published maps and institutional affiliations.